AIP | The Journal of Chemical Physics

# Fast internal dynamics in alcohol dehydrogenase

M. Monkenbusch, A. Stadler, R. Biehl, J. Ollivier, M. Zamponi, and D. Richter

Citation: The Journal of Chemical Physics **143**, 075101 (2015); doi: 10.1063/1.4928512
View online: http://dx.doi.org/10.1063/1.4928512
View Table of Contents: http://scitation.aip.org/content/aip/journal/jcp/143/7?ver=pdfcov
Published by the AIP Publishing



# Fast internal dynamics in alcohol dehydrogenase

M. Monkenbusch,[1] A. Stadler,[1,a)] R. Biehl,[1] J. Ollivier,[2] M. Zamponi,[3] and D. Richter[1]
[1]*Jülich Centre for Neutron Science JCNS and Institute for Complex Systems ICS, Forschungszentrum Jülich GmbH, 52425 Jülich, Germany*
[2]*Institut Laue-Langevin, CS 20156, 38042 Grenoble, France*
[3]*Jülich Centre for Neutron Science JCNS, Forschungszentrum Jülich GmbH, Outstation at MLZ, Lichtenbergstraße 1, 85747 Garching, Germany*

(Received 7 July 2015; accepted 31 July 2015; published online 18 August 2015)

Large-scale domain motions in alcohol dehydrogenase (ADH) have been observed previously by neutron spin-echo spectroscopy (NSE). We have extended the investigation on the dynamics of ADH in solution by using high-resolution neutron time-of-flight (TOF) and neutron backscattering (BS) spectroscopy in the incoherent scattering range. The observed hydrogen dynamics were interpreted in terms of three mobility classes, which allowed a simultaneous description of the measured TOF and BS spectra. In addition to the slow global protein diffusion and domain motions observed by NSE, a fast internal process could be identified. Around one third of the protons in ADH participate in the fast localized diffusive motion. The diffusion coefficient of the fast internal motions is around two third of the value of the surrounding $D_2O$ solvent. It is tempting to associate the fast internal process with solvent exposed amino acid residues with dangling side chains. © *2015 AIP Publishing LLC.* [http://dx.doi.org/10.1063/1.4928512]

## I. INTRODUCTION

Proteins are dynamic objects, which are characterized by motions occurring on different length and time scales. On one hand, amplitudes of motion in biomacromolecules may not be too large as the structure needs to be maintained and stabilized to prevent unfolding at physiological conditions. In protein crystals, for example, the atomic positions can be determined with Å resolution and the salient structural features are kept in solution.[1] On the other hand, it is reasonable to assume that molecular dynamics contributes and even is essential for the biological function of the protein. Flexibility and domain mobility in enzymes are prerequisites for conformational changes that occur in the course of the enzymatic reactions.[2] Weak links between domains may act as analogues to mechanical hinges that allow motions to occur, which enables substrates or cofactors to be incorporated into the protein at the functional sites and to be released after the catalytic reaction. Fast localized motions are equally important for the biological function. Localized fluctuations of any kind in the ns and ps time scale contribute to the conformational entropy of the protein.[3,4] Changes of the conformational entropy induced by substrate binding also contribute to the associated free energy.[3] This may be related to allosteric signalling between different parts of the biomacromolecule.[5] Local dynamics on the ps and ns time scale, in terms of orientational correlation, is accessible and can be investigated by NMR.[6,7] Neutron scattering, on the other hand, is sensitive to the position correlation of atoms. At longer length scales, collective motions of domains[8] or flexible regions[9] can be seen. Locally, the self-correlation of protons dominates the experimental signal.

Alcohol dehydrogenase (ADH) is a protein that catalyzes the interconversion between alcohol and ketones. ADH catalyzes both directions of the conversion from ethanol to acetaldehyde with nicotinamide adenine dinucleotide (NAD) as co-factor. For many organisms, it is essential to use ethanol as a carbon source. Furthermore, ADH enables the detoxification reaction at high alcohol concentrations. ADH is found as a dimer[10] or as a tetramer in *S. cerevisiae*.[11] The tetrameric conformation of yeast ADH shows two crossed dimeric dumbbell like subunits each with two globular monomers, see Figure 1. The monomers have two subdomains separated by a cleft, in which the active site is located. One subdomain hosts the catalytic zinc atom, the other one the NAD co-factor binding site.[2,12]

In a previous neutron spin-echo spectroscopy (NSE) and small-angle neutron scattering (SANS) study, the center-of-mass and rotational diffusion as well as large-scale domain motions in ADH from *S. cerevisiae* could be determined.[8] The $Q$-dependent diffusion $D_{\text{eff}}(Q)$ was obtained from the initial slope of the coherent intermediate scattering functions $S(Q,t)/S(Q)$ that were measured with NSE spectroscopy. An additional contribution $\Delta D_{\text{eff}}(Q)$ on top of the rigid protein rotational and translational diffusion was found, which could be interpreted using normal mode analysis. The normal modes were calculated using an elastic network model.[14] The calculated normal modes serve as trial displacement patterns to compute the form factor of the domain motion effect on $\Delta D_{\text{eff}}(Q)$. The lowest normal modes that best represent the observed wave-vector dependence of $\Delta D_{\text{eff}}(Q)$ imply a cleft opening motion indicating that they may pertain to biological function by opening the access to the catalytic region. NAD incorporation reduces their amplitude. A closer analysis of the time dependence of $S(Q,t)$ at $Q$-values where $\Delta D_{\text{eff}}(Q)$ is largest allows the decomposition of the relaxation into parts from the domain motion and the

a)Electronic mail: a.stadler@fz-juelich.de

 

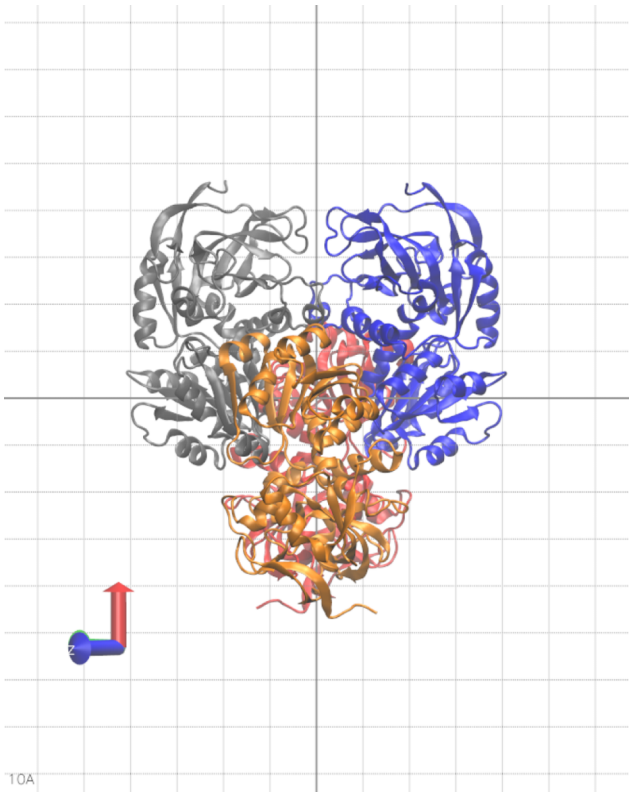


FIG. 1. Representation of the ADH tetramer. The color discriminates the 4 sub-chains. The grid width is 10 Å.[13]

rigid body rotational and translational diffusion contributions. This reveals a characteristic time for the domain relaxation of $\tau_d \simeq 30$ ns after subtraction of the unavoidable background dynamics due to the center-of-mass diffusion and the rotational diffusion.[8]

Following the previous NSE investigation, the same protein was chosen to investigate the more localized dynamics sitting on top of the "background" of the slow motions. In this article, we present a study using neutron time-of-flight (TOF) and backscattering (BS) spectroscopy, which cover a wavevector range from 0.1 $Å^{-1}$ up to 1.8 $Å^{-1}$, looking at length scales from atomic distances to side-chain fluctuations. Most of this range is dominated by the incoherent hydrogen ($^1$H) scattering showing the proton self-correlation in time. On the ps to ns time scale, this implies that protons act as reporters for the motions of larger chemical groups to which they are bound. Part of the dynamics of the hydrogen atoms reflect the motions due to rigid body center-of-mass and rotational diffusion as well as large-scale domain motions as seen in the NSE experiment.[8] In addition to these slow motions, we observe an additional faster and more localized component using TOF and BS spectroscopy.

## II. EXPERIMENTAL

### A. Sample

The sample composition was selected such that it exactly matches that used in the previous SANS and NSE experiments.[8] ADH from *S. cerevisiae* was purchased from Sigma-Aldrich (product number A3263). The ADH powder was dissolved in a buffer solution composed of 10 mM $NaH_2PO_4$/$Na_2HPO_4$, 100 mM NaCl in $D_2O$ with 99.9% atom D at pH 7.5. The freshly prepared protein solution was dialysed against $D_2O$ buffer with an excess volume of 100 in order to virtually remove any exchanged protons from the protein. After the final dialysis step, an aliquot of the dialysate was taken as $D_2O$ reference buffer for the neutron scattering measurements. In order to remove aggregates, the solution was filtered through 0.2 $\mu$m membrane filter and centrifuged at 21 000 g for several hours. The protein concentration was adjusted to 52 mg/ml by buffer dilution assuming an optical extinction coefficient of E1% = 14.6 at 280 nm. The samples of the protein solution as well as for the buffer solution consisted of a row of 20 quartz capillaries with 1.1 mm inner diameter and glass thickness of 0.2 mm, sealed with paraffin wax at the top, which were enclosed in a flat Al-sample holder. This leads to good temperature uniformity, but avoids contamination of the sample with Al ions and also reduces excessive multiple scattering and self-shielding of the sample. It was observed that ADH solution in direct contact with Al showed increased turbidity after 24 h, probably due to the influence of dissolved Al ions. Therefore, from a technical point of view we explored the suitability of thin quartz capillaries as the primary sample container for TOF and BS experiments in this study.

### B. Dynamic light scattering

Monodispersity and absence of aggregates was verified using dynamic light scattering (DLS). The ADH solution with a concentration of 52 mg/ml in $D_2O$ buffer at a temperature of 10 °C was characterized by DLS. The CONTIN analysis[15] of the correlation spectra showed only one single component with 100% intensity. The measured center-of-mass diffusion coefficient was $D_{cm} = 2.75 \pm 0.10$ $Å^2$/ns corresponding to a hydrodynamic radius of $R_h = 4.5 \pm 0.2$ nm, which is identical to previous results for the ADH tetramer.[8] The used solvent viscosity was 1.679 mPas.

### C. Neutron spectroscopy

High resolution neutron TOF and BS spectra have been measured using the instruments IN5[16,17] at the Institut Laue-Langevin, Grenoble, France and SPHERES[18] operated by JCNS at the Heinz Maier-Leibnitz Zentrum, Garching, Germany.

TOF experiments at IN5 have been conducted using a wavelength of $\lambda = 15$ Å yielding an energy resolution of $\Delta\hbar\omega \simeq 4$ $\mu$eV, i.e., $\Delta\omega = 6$ $ns^{-1}$. The covered Q-range was 0.05–0.75 $Å^{-1}$. Prior to further evaluation, the data have been binned into 15 histograms of 1024 time channels, each representing a different $Q$-value (width $\Delta Q = 0.05$ $Å^{-1}$). On IN5 the buffer solution was measured at 5° and 22 °C, the sample at 5 °C. The data collection times for one sample condition were between 12 and 24 h. BS experiments at the instrument SPHERES were conducted at the standard wavelength $\lambda = 6.27$ Å corresponding to the Si[111] reflection. The energy resolution was $\Delta\hbar\omega \simeq 0.7$ $\mu$eV, ($\Delta\omega = 1$ $ns^{-1}$). Scattered neutrons were analysed and focused to 16 detectors

by reflection from large Si-crystal covered mirrors. Thus, the $Q$-range extended from 0.166 Å$^{-1}$–1.8 Å$^{-1}$. On SPHERES, the buffer and the protein solution were measured at 5 °C. In both cases resolution and normalization data were obtained by scattering from a 1 mm vanadium plate at the same size and orientation as the sample.

Transmissions of the protein solution and $D_2O$ buffer with 1 mm thickness were measured on the SANS instrument KWS2 (6.1 Å: $T_{5\%ADH} = 0.9, T_{D2O} = 0.93$; 11.5 Å: $T_{5\%ADH} = 0.88, T_{D2O} = 0.90$; 17.1 Å: $T_{5\%ADH} = 0.86, T_{D2O} = 0.91$;). Data were corrected for self-absorption using the formalism of Paalman and Pings.[19] The measured intensities from the $D_2O$ buffer were weighted by the prefactor $f = 1 - \phi = 0.96$, where $\phi = 52$ mg/ml $\times 0.73$ ml/mg $= 0.04$ is the volume fraction of ADH in the solution. Consequently, the weighted buffer contribution was subtracted from the measured spectra of the protein solution. The buffer subtraction procedure is justified as all exchangeable protons of the protein have been removed during sample dialysis, and the $D_2O$ buffer had exactly the same composition as the solvent of the protein solution. Furthermore, we had shown before that the diffusion of water remains bulk-like even in highly crowded protein solutions.[20] Only water molecules in the first hydration shell (typically in the order of around 0.4 g $D_2O$/g dry protein) show reduced dynamics, but as we are using heavy water the incoherent scattering contribution of that water fraction does not contribute significantly to the measured intensities of the protein solutions.

As shown in Figure 2, the coherent SANS cross section contributes substantial intensity up to quite large momentum transfers. Below $Q \simeq 0.4$ Å$^{-1}$ the scattering still contains significant coherent contributions. Virtually pure incoherent scattering is only observed beyond $Q \simeq 0.4$ Å$^{-1}$.

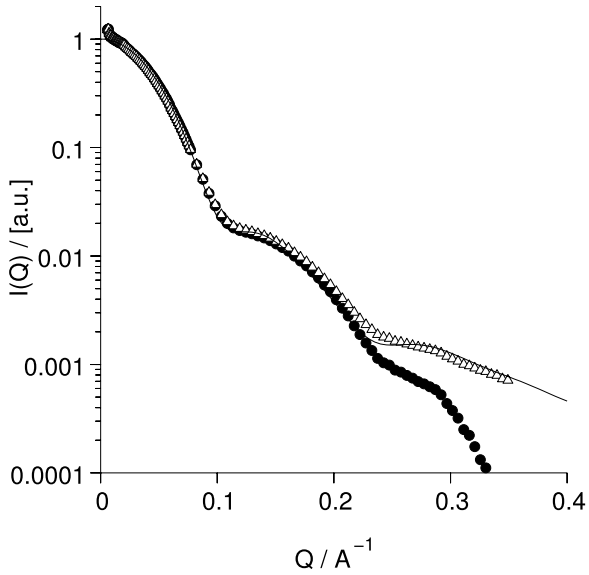


FIG. 2. SANS from the ADH solution. Data correspond to the coherent intensity that had been analyzed using NSE.[8] Solid circles show the intensity after default background subtraction, open triangles are the same data with an empirical offset such that the computed intensities are better matched as corroborated by the TOF intensities (Figure 3). The solid line is the calculated form factor from the tetrameric crystal structure.

## III. SCATTERING INTENSITIES

### A. Elastic scattering

The computed diffusion constants (using HYDROPRO with molecular configuration from the crystal structure) are consistent with the values obtained by DLS and NSE. The diffraction intensity as obtained by SANS or energy-transfer integrated data from TOF reveals the relative amounts of coherent and incoherent scattering. The coherent SANS form factor (Figure 2, see Ref. 8) is close to that computed from the structure of the tetramer inferred from the crystal structure (2hcy). At 5% concentration, the low $Q$-range ($Q < 0.1$ Å$^{-1}$) is somewhat affected by an intermolecular structure factor due to the repulsive interaction between the proteins. At larger momentum transfer, the influence of this structure factor is negligible. The deviations at larger wavevector ($Q > 0.2$ Å$^{-1}$) are probably due to uncertainties in the subtraction of the (incoherent) background. As shown in Figure 3, also the analysis of the $\omega$-integrated spectral intensity from the TOF experiment matches and extends the data on the coherent scattering corresponding to the tetrameric ADH structure, including a constant incoherent contribution at larger $Q$. Up to $Q \simeq 0.4$ Å$^{-1}$, the scattering still contains significant coherent contributions. Virtually pure incoherent scattering is only observed beyond $Q \simeq 0.4$ Å$^{-1}$ corresponding to a "clean" representation of the hydrogen self-correlation, which has been interpreted as described in Secs. IV–VII. As a whole, the crystal structure as tetramer is corroborated and thus may also serve as a basis for the interpretation of the dynamics seen in the incoherent scattering.

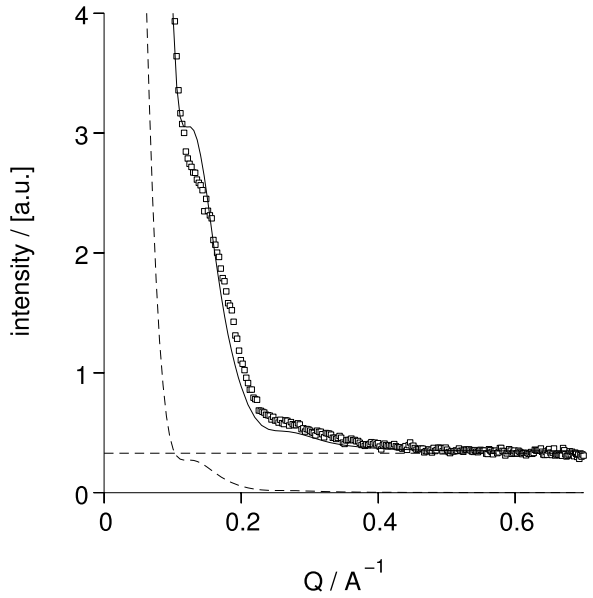


FIG. 3. Integrated intensity (over a 300 ns$^{-1}$ window around the quasi-elastic lines) from the IN5 TOF data set at 5 °C (symbols) compared to the computed SANS intensity assuming the molecular configuration from the tetrameric X-ray crystal structure (solid line computed $S(Q)$ with a constant incoherent contribution added, dashed curve: $S(Q)/10$ to illustrate the strong increase of $S(Q)$ at even smaller Q-values). The dashed horizontal line indicates the incoherent level from the sample (protein protons). It is evident that up to a Q-value of approximately 0.4 Å$^{-1}$ a part of the observed intensity is coherent.

### B. Inelastic scattering

The total scattering intensity of the sample in the incoherent regime ($Q > 0.4$ Å$^{-1}$) contains about 75% background from buffer and empty cell contributions. Hence, the buffer spectrum from exactly the same buffer (as ensured by dialysis) under the same conditions and using the same data collection time had to be measured and was subtracted taking into account the proper self-shielding factors. To evaluate the buffer solution spectra measured on IN5, in particular to check for the diffusion of $D_2O$, empty cell scattering was subtracted. To verify the validity of the procedures, the buffer solution was treated accordingly. After these corrections, a neat quasi-elastic signal due to water diffusion was obtained (mainly caused by the incoherent scattering contribution of D). Fitting of the water diffusion in the $D_2O$-buffer measured on IN5 yields the values 103.1 and 157.2 Å$^2$/ns at 5 and 22 °C, respectively (see Appendix A for details). The measured values are close to the literature values of 104.7 and 159.6 Å$^2$/ns at 5 and 22 °C,[21,22] respectively. Thereby, the whole series of data treatment procedures from binning, subtraction, resolution modelling to fitting the Fourier transforms is validated.

#### 1. Quasielastic contribution

In order to cover a large $(Q, \omega)$-range, high resolution TOF data (IN5) are combined with BS results (SPHERES). The use of $\lambda = 15$ Å for the TOF experiment yields an energy resolution $\Delta\hbar\omega \simeq 4$ $\mu$eV, but on a restricted wave-vector range $0.1 < Q < 0.7$ Å$^{-1}$. Pure incoherent scattering is only obtained for $Q > 0.4$ Å$^{-1}$. The BS data ($\Delta\hbar\omega \simeq 0.7$ $\mu$eV) extend to $Q < 1.8$ Å$^{-1}$, however, with a limited energy range $-22 < \hbar\omega < 22$ $\mu$eV ($-33 < \omega < 33$ ns$^{-1}$). Figure 4 shows the comparison of spectra from ADH at 5 °C with closely matching $Q$-values obtained by TOF and BS, illustrating that BS exhibits a better resolution as seen close to $\omega = 0$, but TOF extends to larger energy transfers with a better statistics. Note that the intensity level at the end of the BS spectrum matches the TOF spectrum without further background subtraction. Figure 5 reveals a main property observed prominently in the quasi-elastic TOF spectra, the scattering from the protein spectra exhibits two well separated dynamical components, a slow component and a fast component. A simple fit with an intermediate scattering function composed of two single exponential components (i.e., two Lorentzians) yields a rate constant 1.7 ns$^{-1}$ for the slow component that is in the range of center-of-mass diffusion plus rotational diffusion of the whole molecule, whereas the fast component with 30 ns$^{-1}$ corresponds to 70% of the deuteron mobility in the $D_2O$ buffer. The fast-to-slow intensity ratio from this very simple fit yields a contribution of 77% slow component.

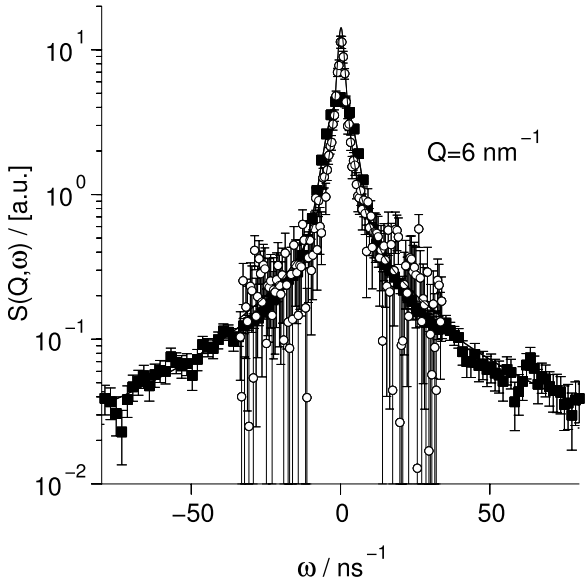


FIG. 4. Comparison of the BS spectrum (open circles) and the TOF spectrum (solid squares) at the overlapping momentum transfer $Q = 0.6$ Å$^{-1}$ at $T = 5$ °C. The BS data have been binned in groups of 4 channels in order to improve statistics. The data have been scaled such that the integral from $-20$ ns$^{-1}$ to 20 ns$^{-1}$ is the same. It is evident that the intensity level at the end of the BS data represents true spectral intensity that matches that from the broader TOF range.

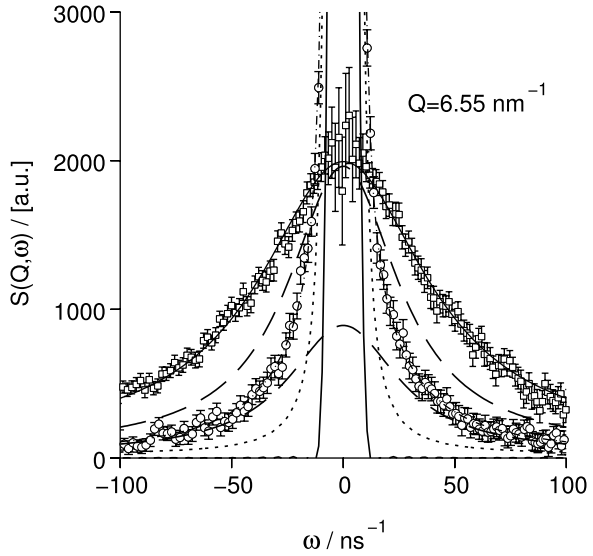


FIG. 5. TOF spectra at $Q = 0.655$ Å$^{-1}$ and $T = 5$ °C comparing the scattering signal from the protons in the protein (circles) with the scattering from the buffer, incoherent scattering of D exhibiting diffusion dynamics of $D_2O$ (squares). Lines indicate the result of simple Lorentzian fits (dashed-dotted: $S(Q,t) = fe^{-t/\tau_1} + (1-f)e^{-t/\tau_2}$) dashed and dotted lines, respectively, represent the fast and slow components. The fast component has been scaled to the level of the buffer diffusion signal (upper dashed line) to allow a comparison of their widths. The Lorentzian fit to the buffer scattering (solid line) yields a relaxation time of $\tau = DQ^2 = 0.023$ ns, i.e., $D = 102$ Å$^2$/ns, which is close to the expected heavy water diffusion constant of 104.7 Å$^2$/ns at 5 °C. The fast component from the protein hydrogen atoms is in the same order of magnitude, but significantly slower than that from the buffer D. The narrow solid line is the measured resolution function.

An analytical model (see Section IV) taking into account center-of-mass and rotational diffusion combined with a component for slow domain motion and a fast contribution describing internal protein dynamics will be used to extract further parameters from the full measured TOF and BS data set.

#### 2. Inelastic contribution

Even if the main focus of the experiment was the observation and analysis of diffusive motions in the quasi-elastic regime, the TOF spectra (on the neutron energy gain side)

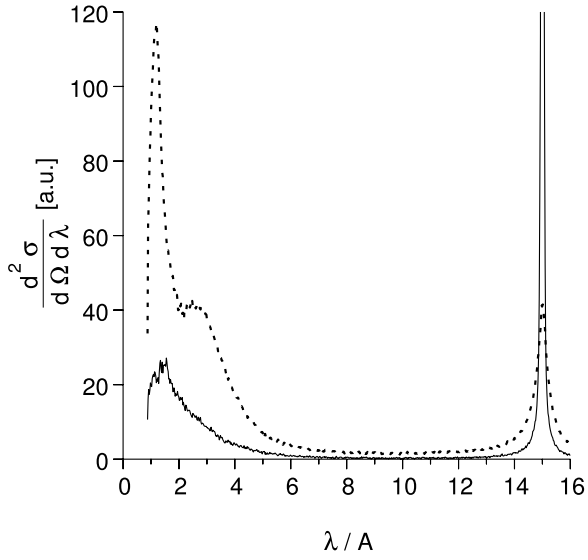


FIG. 6. TOF spectra extending to the limit ($\lambda_f = 1$ Å) of neutron energy gain. The data stem from integrating over the angular range $39° < 2\theta < 113°$. Energy transfers at detected wavelengths of $\lambda = 1, 2, 3, 4, 6$ Å are 81, 20, 8.7, 4.75, 1.9 meV, respectively. Spectra stem from dotted: buffer and solid line: ADH contribution. The temperature was $T = 5$ °C.

extend up to a few times $k_BT$ energy transfer. This is illustrated in Figure 6, where the different contributions from the buffer and the protein are shown separately. Figure 7 displays the inelastic intensity as approximation to the density-of-states analogous to the representation in Lerbret *et al.*[23] Technically, the inspection of the shape differences in the inelastic spectra corroborate the subtraction process, since the ADH spectrum is free from the characteristic peaks from the buffer and the empty cell (empty cell not shown).

Furthermore, we note that a normal solid would show a flat, virtually constant intensity across the elastic line expected for the density of states of acoustic phonons. In contrast, the

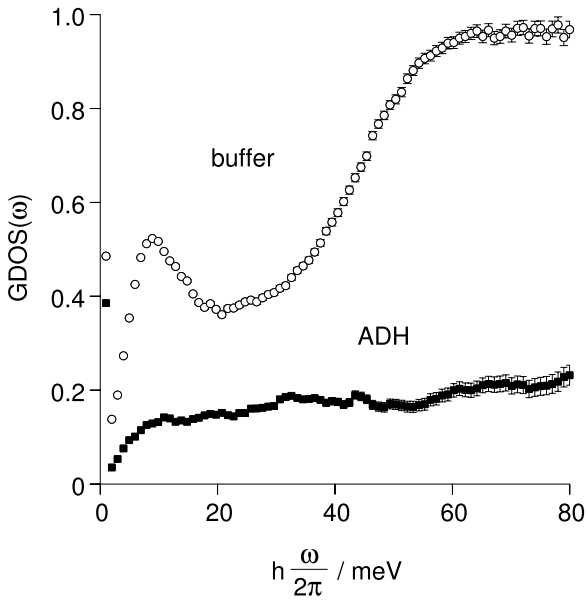


FIG. 7. Generalized density of states as derived from TOF data obtained in the scattering angle range between 20° and 113°. No multi-phonon correction was applied.

protein scattering exhibits a gap between the quasi-elastic part and the inelastic intensity that may be related to the finite size. A coarse estimate of the lowest acoustic mode that fits into an object of $d = 100$ Å size (ADH) assuming a sound velocity of $v = 2000$ m/s would yield a frequency of $\nu \simeq v/d = 2 \times 10^{11}$ s$^{-1}$ and $h\nu = 0.8$ meV, a value corresponding to a final wavelength of $\lambda = 8$ Å. The $D_2O$ buffer spectrum shows two distinct inelastic peak-like structures at about 9 and 55 meV. Both peaks correspond to findings reported by Bellissent-Funel and co-workers,[24,25] and the authors have assigned these features to translational bending modes and librations of water, respectively. However, due to the long wavelength used in this work the larger energy transfer values contain increasing amounts of multiphonon scattering.

Note that none of these features are visible in the inelastic spectrum of solvated ADH corroborating the validity of the subtraction process and thus support the conclusion that the quasi-elastic intensity in the ADH-$D_2O$ buffer difference spectra completely represents the protein hydrogen dynamics. In particular, this shows that the observed fast process in the protein is no artefact due to incomplete buffer subtraction.

## IV. MODELS DESCRIBING QUASIELASTIC SCATTERING

The incoherent quasi-elastic scattering is modelled assuming the following scenario: the whole molecule exhibits translational diffusion with $D_t$ and *isotropic* rotational diffusion $D_r$, the contributions of various hydrogen atoms within the molecule depend on their distance from the center. A fraction of the protons participates additionally in fast internal protein dynamics with respect to rigid body diffusion of the whole molecule. The internal process is in a first approximation modelled as locally confined diffusion.

The convolution with the instrumental resolution is performed by multiplying the time dependent intermediate scattering function corresponding to this model with the Fourier-transform of a representation of the resolution function in the form of a sum of Gaussians (see Appendix B).

Modelling with explicit l-summation for rotational diffusion and confined diffusion in a sphere has been tried (Eqs. (C1)-(C4)), however, they require lengthy summations with very large l-values if the $Q$-range of BS shall be included. That model with l-summation was the basis for a first interpretation of the TOF data.[26] However, the possible contribution of large scale domain motions was neglected in that scenario.

An approach worked out by Volino *et al.*[27] assumes Gaussian confinement and leads to a more efficient formulation by replacing the expression for diffusion in a sphere (Eq. (C3)) with a simpler expression pertaining to a soft confinement such that the proton correlation function is Gaussian. Volino *et al.*[27] compared the behaviour of this approach to the well known expression for diffusion in a sphere, Eq. (C3). Even if the details differ, the salient features of both models match if the radius $R^2 \simeq 5\langle u^2\rangle$ and the diffusion constant inside the sphere relates to the relaxation time of particle correlation $\tau = \langle u^2\rangle / D_s$ towards the Gaussian with width $\sqrt{\langle u^2\rangle}$. The expression for the corresponding intermediate scattering function is then simply[27]

$$F_{\mathrm{gsp}}(Q,t) = \exp\left\{-Q^2u^2[1-e^{-t\,D_s/\langle u^2\rangle}]\right\}. \quad (1)$$

Now this simplified formulation allows the additional incorporation of a large scale domain motion. Assuming that the domain motion alone again corresponds to a Gaussian distribution with a characteristic correlation time $\tau_D$ and a distribution width $\langle a^2\rangle$ that corresponds to the amplitude of the large scale dynamics. The associated motion of the affected hydrogen atoms is considered as one dimensional and its amplitude depends on the location of the hydrogens in the domains. Combining both motions is performed by adding the associated mean square displacements, i.e., in one direction $\langle u^2\rangle(1-\exp[-tD_s/\langle u^2\rangle])$ is replaced by

$$A = \langle u^2\rangle(1-\exp[-tD_s/\langle u^2\rangle]) + \langle a^2\rangle(1-\exp[-t/\tau_D]). \quad (2)$$

With $B = \langle u^2\rangle(1-\exp[-tD_s/\langle u^2\rangle])$, the intermediate scattering function of the combined motion after angular averaging then reads[27]

$$F_{\mathrm{gsp+}}(Q,t) = \frac{\sqrt{\pi}}{2}\,\frac{\mathrm{erf}\left(\sqrt{Q^2(A-B)}\right)\,e^{-Q^2\,B}}{\sqrt{Q^2(A-B)}}. \quad (3)$$

If the domain motion is rather considered to be two-dimensional, the roles of $A$ and $B$ just have to be swapped. Within this model, the overall scattering function is obtained as

$$S_{\mathrm{inc}}(Q,t) = \exp(-D_{\mathrm{cm}}\,Q^2\,t)\sum_{m,n} f_{n,m}\,F_{\mathrm{gsp+}}(Q,A_{m,n}(t),B_{m,n}(t))\,F_{\mathrm{rot}}(Q,r_{1,m},r_{2,m}) \quad (4)$$

instead of Eq. (C4). Where $F_{\mathrm{rot}}$ denotes the Sears expansion given in Eq. (C1), $f_{m,n}$ is the fraction of hydrogens of a class $n$ within shell $m$ with $\sum_m f_{n,m} = f_n$ and $\sum_n f_n = 1$. In principle, the discrimination of different displacement functions $A_{n,m}$ and $B_{n,m}$ would allow to assign position dependent amplitudes to different protons in the molecule, however, it turns out that a very coarse classification in a mobile and a more bound fraction is already sufficient for a description of the data (see Table I). An extra domain motion fraction has also been defined, but has little influence on the fitting due to the relaxation rate virtually beyond the resolution limit.

At larger momentum transfer ($Qr \gg 1$), a further simplification can and must be made by observing that the rotational diffusion part of the hydrogen mean square displacement locally is equivalent to a 2D diffusion with a diffusion constant of $D_{\mathrm{2D,rot}} = D_{\mathrm{rot}}\,r^2$. This means that instead of multiplying with the Sears expansion ($F_{\mathrm{rot}}$ in Eq. (4)), simply the contribution $B_{\mathrm{rot}} = D_{\mathrm{rot}}\,r^2\,t$ has to be added to $B$ in Eq. (4). Thus, the model finally used reads

$$S_{\mathrm{inc}}(Q,t) = \exp(-D_{\mathrm{cm}}\,Q^2\,t)\,\frac{1}{V}\sum_{m=1,n=1}^{N_m,N_n} f_{n,m}\,F_{\mathrm{gsp+}}(Q,A_{m,n}(t),B_{m,n}(t)+D_{\mathrm{rot}}r_m^2t)\,4\pi(r_{2,m}^3-r_{1,m}^3)/3, \quad (5)$$

with $V$ a normalization volume accounting for the summation of rotational diffusion contributions from different shells. The different mobility classes $n$ used are $n = 1$ solid globular part with translational and rotational diffusion only, $n = 2$ outer shell part containing the hydrogen atoms undergoing large scale domain motions, and $n = 3$ fraction of hydrogens that exhibit fast local motions within a range $R^2 \simeq 5\langle u^2\rangle$ with local diffusion coefficient $D_s$. All protons of the different mobility classes participate in rigid body diffusion. For the radius and $Q$-ranges used here the model, Eq. (5), is fully adequate and replaces the explicit models, Eqs. (C1) and (C3), with high accuracy. The advantage is that, e.g., the effect of domain motions can easily be included in Eq. (5) and the necessity to perform summation up to very large orders ($l > 50$) of the spherical harmonics in Eqs. (C1)-(C4) is removed.

In order to complete the description, a small modification of $S(Q,t)$ due to the fact that some protein protons (about 10%) are part of $CH_3$ groups that probably exhibit very fast rotations, a corresponding factor has been applied,[28]

$$S_{\mathrm{inc+}}(Q,t) = S_{\mathrm{inc}}(Q,t)\times\left[(1-f_{\mathrm{CH_3}}) + f_{\mathrm{CH_3}}\left\{EISF + (1-EISF)\,e^{-(t/\tau_{\mathrm{CH_3}})^{\beta}}\right\}\right]$$

with

$$EISF = \frac{1}{3} + \frac{2}{3}\,\frac{\sin(Q\,r_{\mathrm{HH}})}{Q\,r_{\mathrm{HH}}} \quad (6)$$

with the proton-proton jump distance $r_{\mathrm{HH}} = 1.2$ Å, $\tau \simeq 1$ ps, and $\beta = 0.8$.

## V. RESULTS

The three component model, Eq. (5), with the free fitted parameters given in Table I has been applied to the available quasi-elastic spectra beyond $Q = 0.4$ Å$^{-1}$ from both instruments. The first component of the model accounts for rigid body diffusion of the whole protein without visible internal protein dynamics, the second component corresponds to a large-scale domain motion, and the third component represents a fast localised diffusive process. The hydrogen atoms of ADH are divided in three classes belonging to the three components. The double sum in Eq. (5) runs over the three classes of hydrogen atoms and additionally over the different shells of the protein for the calculation of the rotational diffusion. The fractions of the hydrogen atoms belonging to the three types of motion are represented by the proportions $f_1$, $f_2$, and $f_3$, respectively. The fractions $f_1$, $f_2$, and $f_3$ are free parameters. Domain motion is described by the relaxation time $\tau_{\mathrm{D}}$ and the

TABLE I. Fitted model parameters used to describe the TOF and BS data: fractions of hydrogen atoms participating in the different classes of motion, confinement radius, and diffusion coefficient of the fast component.

| Parameters | Three component model | Two component model | Estimated errors |
|---|---|---|---|
| $f_1$ | 0.42 | 0.63 | 0.05 (0.02) |
| $f_2$ | 0.24 | ... | (0.02) |
| $f_3$ | 0.34 | 0.37 | 0.05 (0.01) |
| $R$ | 7.5 Å | 7.1 Å | −1.5 + 3 (0.3) |
| $D_s$ | 78 Å$^2$/ns | 65 Å$^2$/ns | 15 (2) |

amplitude $a$. The relaxation time was fixed to $\tau_D = 30$ ns and the amplitude to $a = 8.4$ Å as measured by NSE.[8] The fast component is characterized by the confinement radius $R$ (or the corresponding RMSD with $\sqrt{\langle u^2 \rangle} = R/\sqrt{5}$) and the diffusion coefficient $D_s$. Both parameters $R$ and $D_s$ were fitted. The internal motions, therefore, are sitting on top of the center-of-mass and rotational diffusion of the whole molecule.

The center-of-mass diffusion $D_{cm}$ and the rotational diffusion $D_r$ have been taken from the NSE experiments.[8] Their values had been derived from DLS results and predictions by HYDROPRO[29] and further corroborated by the NSE results. The effective diffusion constant at finite concentration $D_{cm} = D_0 H(Q)/S_{ip}(Q)$ depends on the inter-particle structure factor $S_{ip}(Q)$ and on the hydrodynamic factor $H(Q)$.[30] Whereas the structure factor is expected to be 1 in the Q-range used here, the hydrodynamic factor is constant but smaller than one. The value of $H(Q)$ at a concentration of 5% as used here and in the NSE investigation turns out to be 0.85. The center-of-mass diffusion, therefore, was fixed to $D_{cm} = 0.85 \times D_0 = 0.85 \times 2.3$ Å$^2$/ns = 1.995 Å$^2$/ns, the rotational diffusion was 0.000 79 ns$^{-1}$.

ADH has a spherical shape with a water filled cavity in its center. The radius of the water filled cavity is $r_{i,1} = 15$ Å. The maximal diameter of ADH is 100 Å. For the calculation of rotational diffusion without additional dynamics, the outer radius of the protein was chosen as $r_{o,1} = 50$ Å. For the calculation of domain motions including rotational diffusion, an inner radius of $r_{i,2} = 40$ Å and an outer radius of $r_{o,2} = 50$ Å were used. The calculation for fast internal dynamics and rotational diffusion was performed between $r_{i,3} = 40$ Å and $r_{o,3} = 50$ Å. The number of supporting points in the summation over the shells was chosen sufficiently large (10 equidistant shells) to provide a good coarse-grained representation of the protein.

The measured TOF and BS spectra with the fitted three component model using the free and fixed parameters described above is shown in Figure 8. Values with specified

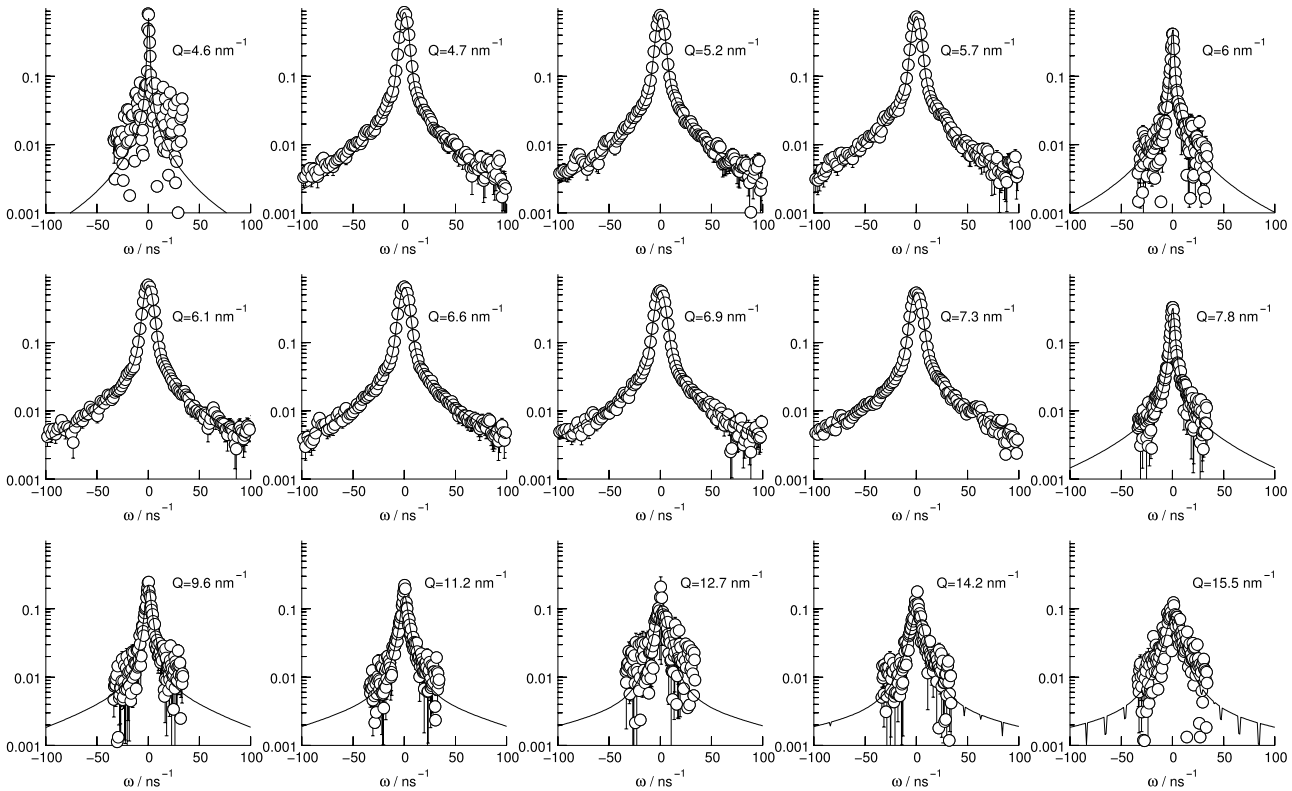


FIG. 8. A compilation of BS (spanning $\omega = \pm 35$ ns$^{-1}$) and TOF spectra with wider $\omega$-range and less resolution over the Q-range covered by both experiments. At the lowest Q-value, no sizeable coherent contribution was observed. The lines through the data represent a fit with the three component model including large-scale domain motion as described in the text. Note that the fit was simultaneous with a common intensity scale with respect to the vanadium spectra. The backscattering data are shown in a version with 4 energy channels binned to improve the statistics.

(statistical) errors were fitted. A simultaneous fit including TOF spectra in the $Q$-range between 0.45 and 0.7 Å$^{-1}$ and $-80 < \omega < 80$ ns$^{-1}$ and the BS spectra from 0.46 to 1.55 Å$^{-1}$ was performed. Using the error bars of counting statistics, the fit of the three component model yields $\chi^2 = 1.34$.

To check for the influence of the domain motion to the measured spectra, the contribution $f_2$ was set to zero meaning that the domain motion is not discernible in the model function. The results of the two component model are compared to the three component model in Table I. The contribution of the domain motion has quasi no effect on the results of the fit, because the time scale of 30 ns is marginal for the spectral resolution of the used TOF and BS instruments. For the two component model $\chi^2 = 1.42$ is obtained, which is only slightly larger than the $\chi^2$ from the more complex three component model. The measured spectra with the fitted two component model are presented in Figure 9. The shell model approach is also rather insensitive to the choice of the inner radii $r_{i,2}$ and $r_{i,3}$, e.g., even by choosing $r_{i,3} = 15$ Å the values for the confinement radius, the diffusion coefficient and the fraction of hydrogen atoms undergoing the fast dynamics remain the same within the errors.

The error values in brackets in Table I are the result of the formal error analysis by the fit procedure. The indicated parameters have been determined by a simultaneous fit where a common intensity scale was used. As illustrated in Figures 8 and 9, a very good data description over the whole $Q$ range is achieved for both models. The resulting parameters, however, are less well defined than the formal statistical error analysis indicates. The larger values are estimates obtained by explicitly changing the parameters until $\chi^2$ is increased by 5%. Knowing the sources of systematic errors (e.g., self-shielding) the latter measure in combination with a visual inspection of the fits appears to give a more realistic error estimate.

However, a stable feature is the presence of the fast component from a locally confined motion with a significantly reduced diffusion coefficient as compared to the $D_2O$ molecules in the surrounding buffer. Prior to the present analysis, the IN5 data alone were also subjected to a fit to the explicit summed Dianoux-Volino model Eq. (C3).[26] There, a confinement radius of $R = 8.3$ Å and a local diffusion of $D_s = 88$ Å$^2$/ns was found, which is close to our present values. Our result concerning the amplitude of localized internal motions in ADH is close to the confinement radius of 6.7 Å for internal dynamics in $\gamma$-globulin[31] and pepsin[32] at pH 5.5 and pH 8 with reported confinement radii of 5.8 Å and 6.6 Å, respectively, measured by high-resolution neutron BS spectroscopy in solution. The equivalent RMSDs of the confinement radii amount to $\sqrt{\langle u^2 \rangle} = R/\sqrt{5} = 3.4$ Å (3 component model) and 3.2 Å (2 component model). The MSDs and diffusion coefficients of the three and two component model yield the relaxation times $\tau = \langle u^2 \rangle / D_s \simeq 0.14$ ns and $\tau = 0.16$ ns, respectively. The fraction $f_3$ of visible non-exchanged protons undergoing the fast localized motion is close to one third for both the two and the three component models.

Note that the observation of this fast local component is the main new feature of internal ADH dynamics that we found.

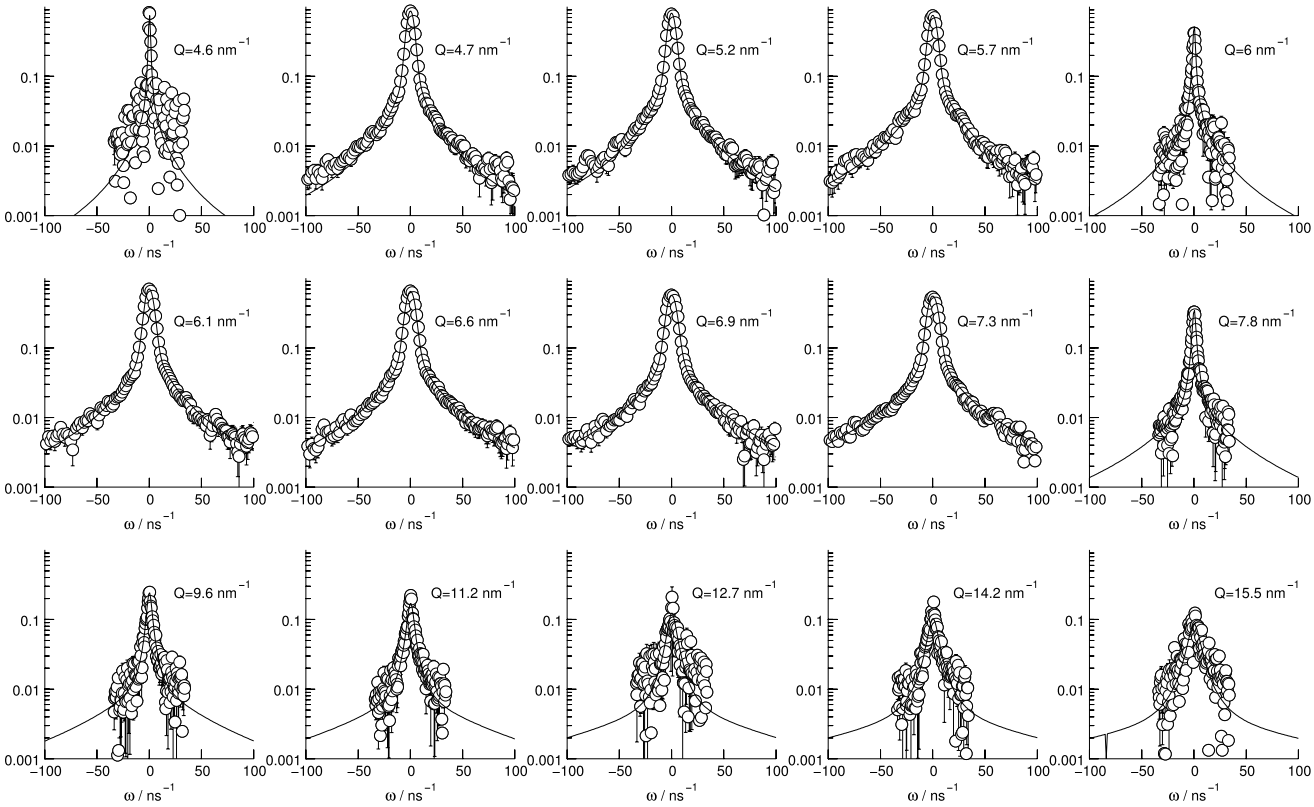


FIG. 9. Measured BS and TOF spectra. The lines through the data represent a fit with the simpler two component model without the large-scale domain motion. The quality of the fit with the two component model is quasi-indistinguishable from the three component fit. Note that the fit was simultaneous with a common intensity scale with respect to the vanadium spectra.

## VI. DISCUSSION

Beyond the corroboration of the global dynamics known from the analysis of coherent scattering from previous NSE experiments at low $Q$, the present study reveals that $f_3 = 34\%$ (three component model) to 37% (two component model) of the hydrogen atoms that are contained in the amino-acids of ADH exhibit a fast dynamics with a typical time scale on the order of 0.14–0.16 ns, whereas the other hydrogen atoms just follow the global motions plus eventual high frequency vibrational type displacements. The initial movement of the observed fast mobile hydrogen atoms resembles diffusion. The obtained diffusion coefficient of internal dynamics is significantly slower than the diffusion of the surrounding $D_2O$ buffer. However, the range of the internal motion in ADH is restricted. This is intuitively clear as the hydrogen atoms are located within amino acid side chains, which are chemically bound to the protein backbone.

The theoretical shell model suggests that hydrogen atoms with fast internal dynamics are close to the surface of ADH, whereas hydrogens without visible internal dynamics are located mainly in the hydrophobic core. To visualize the possibly involved amino acids, we calculated the solvent accessible surface area of all amino acids of the ADH tetramer (pdb code 2hcy) using the MMTK toolkit.[33] A group of residues close to the surface of the protein was determined by choosing a certain cutoff value and selecting the amino acids, which have an accessible surface area larger than the cutoff value. The fraction of surface hydrogens was then defined as the number of hydrogen atoms in the selected amino acid group divided by the total number of hydrogens in ADH. Using that approach, we found that a cutoff value of 0.16 $nm^2$/atom yields a 37% fraction of hydrogen atoms in the surface layer, which agrees with the dynamically mobile $f_3 = 37\%$ fraction identified by neutron scattering using the two component model. The selected surface residues are visualized in Figure 10. The thickness of the selected surface layer is in the order of 1 nm being in agreement with the used inner and outer radius of the shell model. The surface residues selected according to the mobile fraction of the three component model are essentially identical to those shown in Figure 10.

The interpretation of the observed fast amino acids in ADH—but without being a direct proof—is that the surface hydrogens with contact to the surrounding solvent water (see Figure 10) exhibit a fast mobility with a diffusion coefficient being 63% (two component model) to 76% (three component model) than that of bulk $D_2O$ solvent at the same temperature. The buried hydrogen atoms, therefore, would appear as immobile and follow the global movements of the protein domains. Incoherent neutron scattering is equally sensitive to all hydrogen atoms in the sample. Thus, only the dynamic difference allows the classification between immobile and mobile hydrogen atoms. A similar interpretation has been given for the fraction of fast mobile hydrogen atoms observed by TOF spectroscopy with lower energy resolution (around 100 $\mu$eV) in hydrated protein powders and highly concentrated protein solutions.[34,35] In those studies, even faster internal processes with relaxation times in the range of around 10 ps have been detected.[34,35] The results presented in our study are based on a combined interpretation of high-resolution TOF (resolution 4 $\mu$eV) and BS (0.7 $\mu$eV) QENS data. Due to the high energy resolution, internal processes with a relaxation rate of around 0.14–0.16 ns have been in the focus of the neutron spectrometers.

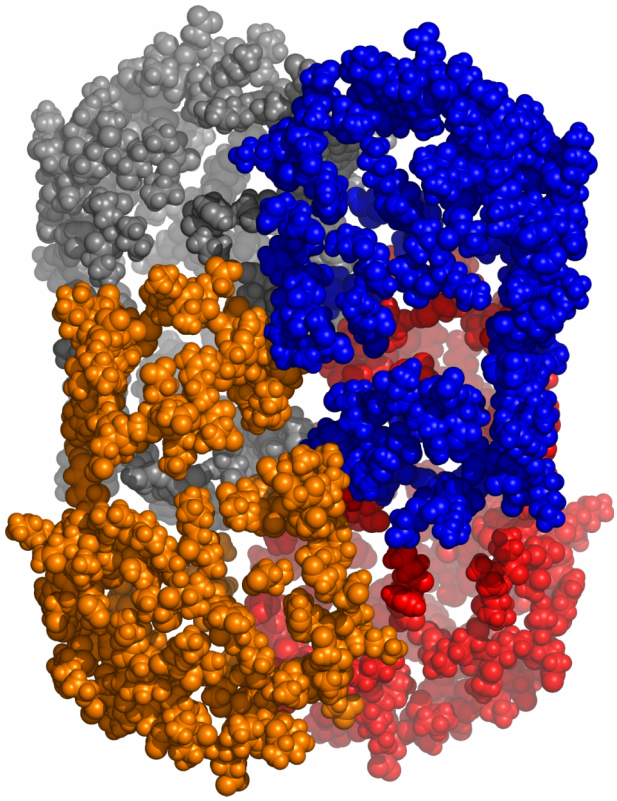

FIG. 10. Surface residues of the ADH tetramer possibly contributing to the mobile fraction observed by neutron scattering. The color discriminates the four domains.

While hydrogen displacements cause the signal seen by incoherent neutron scattering, NMR methods are used to identify protein parts in the backbone[6] or side groups[7] that exhibit reorientational fluctuations within the ps to ns time scale. The derived order parameter is (empirically) related to an entropy contribution, which may contribute significantly to free energy differences upon configurational changes or binding of substrates.[1,5] Due to the connectivity by chemical bonds within the protein, displacements and reorientations are coupled. Thus, a connection between hydrogen atoms showing fast position self-correlation dynamics (seen by incoherent neutron scattering) and large reorientational fluctuations (detected by NMR) can be assumed. However, to our knowledge until now no such investigation on ADH has been performed. The large molecular mass that increases the difficulty for NMR analysis is beneficial for neutron scattering investigations, since global protein diffusion is dynamically well separated from the more localized internal fluctuations. Neutrons have no intrinsic site specificity, which often is an advantage as all kinds of structures or motions contribute to the scattering intensity. However, in the case of large proteins a straightforward discrimination of, e.g., side-group from backbone signal or exposed from buried location is not contained in the signal. Partial deuteration of the protein would help to get positional information.

## VII. CONCLUSION

In summary, a theoretical representation of the dynamics of ADH in solution that is consistent with the previous NSE investigation[8] is presented. On top of the slow motions, which relate to rigid-body diffusion of the whole molecule and large-scale domain motion, around one third of the protons exhibit a fast localized diffusive process. The contribution of the domain motion, however, is barely visible in the measured incoherent spectra, because the time scale of the domain motion is marginal for the spectral resolution of the used TOF and BS spectrometers. The fast internal process is characterized by a diffusion coefficient being significantly slower than the value of the surrounding $D_2O$ solvent. Averaged over all mobile protons, this motion is restricted to a confinement radius of around 7.1 Å (RMSD 3.2 Å). It is tempting to associate the fast moving protons with dangling solvent exposed side-groups. Further investigations on the effect of co-factor binding on the local dynamics are under way.

## ACKNOWLEDGMENTS

This work is based upon experiments performed at the instrument IN5 at the Institut Laue-Langevin (ILL), Grenoble, France and at the instrument SPHERES operated by JCNS at the Heinz Maier-Leibnitz Zentrum (MLZ), Garching, Germany.

## APPENDIX A: BUFFER SCATTERING

The scattering from the buffer dominantly results from the incoherent scattering cross section of deuterons in $D_2O$, which is about 2.5% of the incoherent proton cross section. The quasi-elastic scattering can be perfectly fitted with a single Lorentzian, the $Q$-dependent rates yielding the diffusion coefficient, see Figure 11.

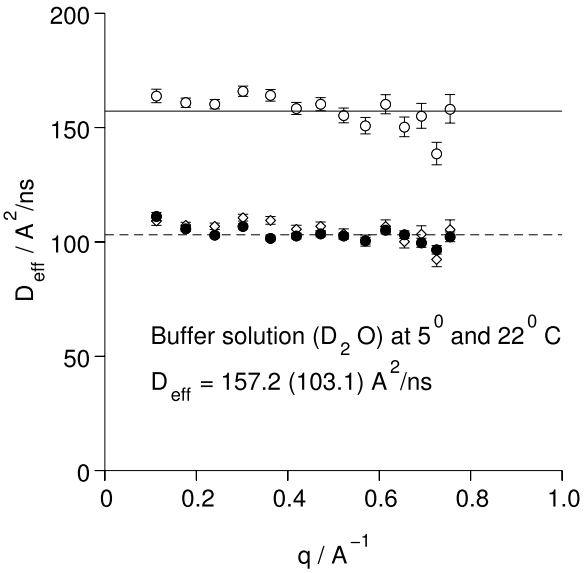


FIG. 11. Diffusion of $D_2O$ in the buffer as determined by single exponential (Lorentz) fits to the buffer background spectra of the TOF experiment. Solid symbols: $T = 5\,°C$, open symbols: $T = 22\,°C$. The high temperature data can be scaled to match the low temperature values by the division factor 1.5. In the covered low $Q$-regime, simple constant diffusion with values that match the literature values[21,22] is observed.

## APPENDIX B: RESOLUTION CONVOLUTION

Model fitting was performed with intermediate scattering functions $S(Q,t)$ specified in the time-domain. To account for the spectrometer resolution and to perform the transformation to the frequency domain, the method used relies on a representation of the resolution function in terms of Gaussians

$$\mathcal{R}(Q,\omega) = \sum_{i=1}^{N} a_i\, e^{-(\omega-\omega_i)^2/w_i^2}. \tag{B1}$$

The parameters $a_i$, $\omega_i$, and $w_i$ as well as the required size of $N$ (in the present case typically 1–4) are determined by fitting of the reference vanadium spectra. The resolution function can be written in terms of Fourier transforms,

$$\mathcal{R}(Q,\omega) = \sum_{i=1}^{N} \int \frac{a_i\, e^{-(w_i\, t)^2/4}}{2\pi^{3/2}\, w_i} \cos([\omega-\omega_i]\, t)dt, \tag{B2}$$

the components of this Gaussian representations decay fast in the time domain enabling an efficient and accurate numerical Fourier-transform integration of the intermediate structure factor $S(Q,t)$ over a finite time domain,

$$I(Q,\omega) = \sum_{i=1}^{N} \int_0^{t_{\max}=W_t/w_i} \frac{a_i\, e^{-(w_i\, t)^2/4}}{2\pi^{3/2}\, w_i} \times \cos([\omega-\omega_i]\, t)\, S(Q,t)\, dt. \tag{B3}$$

In order to avoid errors associated with function of a width in the order or even less than the width of a frequency bin of the histogrammed spectrum the used method is lightly expanded by fitting the resolution with the integral of the Gaussian representation, Eq. (B1), over the bin width $\sum_{i=1}^{N} a_i\{\sqrt{\pi/4}\, w_i/\delta\omega\} \times (\mathrm{erf}([2\omega+\delta\omega]/2w_i) - \mathrm{erf}([2\omega-\delta\omega]/2w_i))$. And then computing the intensity to be fitted $I(Q,\omega)$ using the same integration over a bin width by replacing Eq. (B3) with

$$I(Q,\omega) = \sum_{i=1}^{N} \int_0^{t_{\max}=W_t/w_i} \frac{a_i\, e^{-(w_i\, t)^2/4}}{2\pi^{3/2}\, w_i} \frac{\sin(\{-[\omega-\omega_i]+\delta\omega/2\}\, t) + \sin(\{[\omega-\omega_i]+\delta\omega/2\}\, t)}{t\,\delta\omega} S(Q,t)\, dt. \tag{B4}$$

Thus, spectral features with structure within the bin width of the histogram are treated properly. For the typical intermediate scattering functions $S(Q,t)$, the implied numerical Fourier-integration can efficiently be executed using an adaptive method. There are no cutoff effects or the typical fast Fourier transform artifacts.

The fit shown in this paper is obtained with this method of resolution convolution, where $S(Q,t)$ is described in Sec. IV.

## APPENDIX C: MODELS WITH EXPLICIT L-SUMMATION

For the rigid body contribution, the center-of-mass diffusion combined with rotational diffusion contributions computed by the Sears expansion[36] yields the intermediate scattering function

$$F_{diro}(Q,t,r_1,r_2) = \exp(-D_{\rm cm}\,Q^2 t) \times \sum_m f_m \underbrace{\sum_l^{l_{\max}} (2l+1) A_l(Q,r_{1,m},r_{2,m})\, e^{-l(l+1)D_r\, t}}_{F_{\rm rot}(Q,r_{1,m},r_{2,m})}, \tag{C1}$$

with $f_m$ the fraction of protons in shell $m$ from $r = r_{1,m} \cdots r_{2,m}$ distance from the center. $D_{\rm cm}$ denotes the center of mass diffusion and $D_r$ the rotational diffusion constant,

$$A_n(Q,r_1,r_2) = \int_{r_1}^{r_2} j_n(Qr)^2\, r^2\, dr \Big/ \int_{r_1}^{r_2} r^2\, dr. \tag{C2}$$

A fraction of the protons with additional mobility are modeled by diffusion in spheres of radius $R$ that are attached at some point of the "rigid" protein. The expression of Volino and Dianoux for diffusion inside a sphere[37] describes the intermediate scattering contribution

$$F_{\rm dsph}(Q,t,R) = \left(\frac{3j_1(QR)}{QR}\right)^2 + 6 \sum_{(l,\nu)\neq 0}^{(l,\nu)_{\max}} \left[\frac{QR\, j_{l+1}(QR) - l\, j_l(QR)}{(QR)^2 - z_{l,\nu}^2}\right]^2 \frac{(2l+1) z_{l,\nu}^2}{z_{l,\nu}^2 - l(l+1)}\, e^{-z_{l,\nu}^2\, D_s/R^2\, t}, \tag{C3}$$

with $z_{l,\nu}$ the zeros of the equation $0 = j_l(z) - z\, j_{l+1}(z)$, typical values that must be used for the large protein are $l_{\max} = 30$–$40$ and $z_{\max} = 30$. For the $Q$-range of the backscattering spectrometer, even larger $l$-values would be needed. Finally the combined model assuming restricted additional proton motions in some shells of the globule reads

$$S_{\rm inc}(Q,t) = \exp(-D_{\rm cm}\,Q^2 t) \sum_m f_m \left[(1-\phi_m) + \phi_m F_{dsph}(Q,t,R)\right] \sum_l^{l_{\max}} (2l+1) A_l(Q,r_{1,m},r_{2,m})\, e^{-l(l+1)D_r\, t}, \tag{C4}$$

where $\phi_m$ denotes the fraction of mobile protons in shell $m$ and $\sum_m f_m = 1$.

This model was the basis for a first inspection of TOF data.[26]


[1]K. Henzler-Wildman and D. Kern, "Dynamic personalities of proteins," Nature **450**, 964–972 (2007).

[2]S. Hammes-Schiffer and S. J. Benkovic, "Relating protein motion to catalysis," Annu. Rev. Biochem. **75**, 519–541 (2006).

[3]K. K. Frederick, M. S. Marlow, K. G. Valentine, and A. J. Wand, "Conformational entropy in molecular recognition by proteins," Nature **448**, 325–329 (2007).

[4]A. M. Stadler, M. M. Koza, and J. Fitter, "Determination of conformational entropy of fully and partially folded conformations of holo- and apomyoglobin," J. Phys. Chem. B **119**, 72–82 (2015).

[5]S.-R. Tzeng and C. G. Kalodimos, "Protein activity regulation by conformational entropy," Nature **488**, 236–240 (2012).

[6]V. Jarymowycz and M. Stone, "Fast time scale dynamics of protein backbones: NMR relaxation methods, applications, and functional consequences," Chem. Rev. **106**, 1624–1671 (2006).

[7]T. Igumenova, K. Frederick, and A. Wand, "Characterization of the fast dynamics of protein amino acid side chains using NMR relaxation in solution," Chem. Rev. **106**, 1672–1699 (2006).

[8]R. Biehl, B. Hoffmann, M. Monkenbusch, P. Falus, S. Preost, R. Merkel, and D. Richter, "Direct observation of correlated interdomain motion in alcohol dehydrogenase," Phys. Rev. Lett. **101**, 138102 (2008).

[9]A. M. Stadler, L. Stingaciu, A. Radulescu, O. Holderer, M. Monkenbusch, R. Biehl, and D. Richter, "Internal nanosecond dynamics in the intrinsically disordered myelin basic protein," J. Am. Chem. Soc. **136**, 6987–6994 (2014).

[10]F. Colonna-Cesari, D. Perahia, M. Karplus, H. Eklund, C. I Brändén, and O. Tapia, "Interdomain motion in liver alcohol dehydrogenase: Structural and energetic analysis of the hinge bending mode," J. Biol. Chem. **261**, 15273–15280 (1986).

[11]S. Ramaswamy, D. Kratzer, A. Hershey, P. Rogers, A. Arnone, H. Eklund, and B. Plapp, "Crystallization and preliminary crystallographic studies of saccharomyces-cerevisiae alcohol dehydrogenase-I," J. Mol. Biol. **235**, 777–779 (1994).

[12]E. Negelein and H. Wulff, "Diphospho-pyridin proteid, alcohol and acetaldehyde," Biochem. Z. **293**, 351–389 (1937).

[13]W. Humphrey, A. Dalke, and K. Schulten, "Vmd: Visual molecular dynamics," J. Mol. Graphics **14**, 33 (1996).

[14]K. Suhre and Y. Sanejouand, "Elnemo: A normal mode web server for protein movement analysis and the generation of templates for molecular replacement," Nucleic Acids Res. **32**, W610–W614 (2004).

[15]S. Provencher, "Contin: A general purpose constrained regularization program for inverting noisy linear algebraic and integral equations," Comput. Phys. Commun. **27**, 229 (1982).

[16]J. Ollivier, M. Plazanet, H. Schober, and J. Cook, "First results with the upgraded IN5 disk chopper cold time-of-flight spectrometer," Phys. B **350**, 173–177 (2004).

[17]J. Ollivier and H. Mutka, "In5 cold neutron time-of-flight spectrometer, prepared to tackle single crystal spectroscopy," J. Phys. Soc. Jpn. **80**(Suppl. B), SB003 (2011).

[18]J. Wuttke, A. Budwig, M. Drochner, H. Kämmerling, F.-J. Kayser, H. Kleines, V. Ossovyi, L. C. Pardo, M. Prager, D. Richter, G. J. Schneider, H. Schneider, and S. Staringer, "SPHERES, Jülich's high-flux neutron backscattering spectrometer at FRM II," Rev. Sci. Instrum. **83**, 075109 (2012).

[19]H. H. Paalman and C. J. Pings, "Numerical evaluation of x-ray absorption factors for cylindrical samples and annular sample cells," J. Appl. Phys. **33**, 2635–2639 (1962).

[20]A. M. Stadler, J. P. Embs, I. Digel, G. M. Artmann, T. Unruh, G. Bldt, and G. Zaccai, "Cytoplasmic water and hydration layer dynamics in human red blood cells," J. Am. Chem. Soc. **130**, 16852–16853 (2008).

[21]L. G. Longsworth, "The mutual diffusion of light and heavy water," J. Phys. Chem. **64**, 1914–1917 (1960).

[22]Y. Edura and N. Morishima, "Cold and thermal neutron scattering in liquid water - II: Scattering laws and group constants for $H_2O$ and $D_2O$," Nucl. Instrum. Methods Phys. Res., Sect. A **545**, 309–318 (2005).

[23]A. Lerbret, A. Hedoux, B. Annighoefer, and M.-C. Bellissent-Funel, "Influence of pressure on the low-frequency vibrational modes of lysozyme

and water: A complementary inelastic neutron scattering and molecular dynamics simulation study," Proteins: Struct., Funct., Bioinf. **81**, 326–340 (2013).
[24]M. Bellissent-Funel and J. Teixeira, "Dynamics of water studied by coherent and incoherent inelastic neutron-scattering," J. Mol. Struct. **250**, 213–230 (1991).
[25]M. Bellissent-Funel, S. Chen, and J. Zanotti, "Single-particle dynamics of water-molecules in confined space," Phys. Rev. E **51**, 4558–4569 (1995).
[26]A. Stadler, M. Monkenbusch, R. Biehl, D. Richter, and J. Ollivier, "Neutron spin-echo and TOF reveals protein dynamics in solution," J. Phys. Soc. Jpn. **82**, SA016 (2013).
[27]F. Volino, J.-C. Perrin, and S. Lyonnard, "Gaussian model for localized translational motion: Application to incoherent neutron scattering," J. Phys. Chem. B **110**, 11217–11223 (2006).
[28]M. Bée, *Quasielastic Neutron Scattering* (Adam Hilger, 1988).
[29]J. de la Torre, M. Huertas, and B. Carrasco, "Calculation of hydrodynamic properties of globular proteins from their atomic-level structure," Biophys. J. **78**, 719–730 (2000).
[30]W. Hess and R. Klein, "Generalized hydrodynamics of systems of Brownian particles," Adv. Phys. **32**, 173–283 (1983).
[31]M. Grimaldo, F. Roosen-Runge, F. Zhang, T. Seydel, and F. Schreiber, "Diffusion and dynamics of $\gamma$-globulin in crowded aqueous solutions," J. Phys. Chem. B **118**, 7203–7209 (2014).
[32]D. R. Dee, B. Myers, and R. Y. Yada, "Dynamics of thermodynamically stable, kinetically trapped, and inhibitor-bound states of pepsin," Biophys. J. **101**, 1699–1709 (2011).
[33]K. Hinsen, "The molecular modeling toolkit: A new approach to molecular simulations," J. Comput. Chem. **21**, 79–85 (2000).
[34]J.-M. Zanotti, M.-C. Bellissent-Funel, and J. Parello, "Hydration-coupled dynamics in proteins studied by neutron scattering and nmr: The case of the typical ef-hand calcium-binding parvalbumin," Biophys. J. **76**, 2390–2411 (1999).
[35]A. M. Stadler, C. J. Garvey, J. P. Embs, M. M. Koza, T. Unruh, G. Artmann, and G. Zaccai, "Picosecond dynamics in haemoglobin from different species: A quasielastic neutron scattering study," Biochim. Biophys. Acta, Gen. Subj. **1840**, 2989–2999 (2014).
[36]V. Sears, "Theory of cold neutron scattering by homonuclear diatomic liquids. 2. Hindered rotation," Can. J. Phys. **44**, 1299 (1966).
[37]F. Volino and A. Dianoux, "Neutron incoherent-scattering law for diffusion in a potential of spherical-symmetry - general formalism and application to diffusion inside a sphere," Mol. Phys. **41**, 271–279 (1980).